ELSEVIER

Journal of Organometallic Chemistry 571 (1998) 123–128

Journal of Organo metallic Chemistry

Iron/gold carbide clusters containing Fe_5Au or Fe_5Au_2 skeletons: X-ray crystal structure of $[Fe_5CAu_2(CO)_{14}(dppm)]$

Oriol Rossell [a,1], Miquel Seco [a], Glòria Segalés [a], Maria Angela Pellinghelli [b], Antonio Tiripicchio [b,*]

[a] *Departament de Química Inorgànica, Universitat de Barcelona, Martí i Franquès 1, E-08028 Barcelona, Spain*
[b] *Dipartimento di Chimica Generale ed Inorganica, Chimica Analitica, Chimica Fisica, Università di Parma, Centro di Studio per la Strutturistica Diffrattometrica del CNR, Viale delle Scienze 78, I-43100 Parma, Italy*

Received 22 June 1998

Abstract

The reaction of $(NEt_4)_2[Fe_5C(CO)_{14}]$ with $(AuCl)_2$(diphos) depends on the stoichiometry of the process. Thus, with a 1:1 molar ratio, the cluster $[Fe_5CAu_2(CO)_{14}$(diphos)] (diphos = dppm, **1**; dppe, **2**; dppp, **3**) was obtained. The X-ray crystal structure of **1** revealed that the metal core can be described as a square-based pyramid of Fe atoms and a trigonal bipyramid, with two Fe and one Au atoms at the vertices of the base and one Au and one Fe atoms at the apices, sharing a triangular face of Fe atoms. However, the use of a 2 (iron anion):1 (gold derivative) molar ratio yielded the cluster $(NEt_4)_2[\{Fe_5CAu(CO)_{14}\}_2$(diphos)] (diphos = dppm, **4**; dppe, **5**; dppp, **6**), in which two octahedral Fe_5Au metal cores are linked by the diphosphine. On reacting with $ClAuPR_3$, the latter derivative underwent an unusual ligand redistribution process. © 1998 Elsevier Science S.A. All rights reserved.

Keywords: Electrophilic addition; Carbide clusters; Gold and iron fragments

1. Introduction

The reaction of anionic metal carbonyl clusters with gold–phosphine fragments to form heterometallic clusters is well known. Although the use of bimetallic or trimetallic cationic fragments of gold has been less studied [1], the $[Au_2(diphos)]^{2+}$ fragments have been proved remarkably versatile. Not only the gold atoms can act in a μ_n ($n = 1$–4) bonding manner, but the $[Au_2(diphos)]^{2+}$ unit can be bound to a cluster anion through the two gold atoms or can link two cluster units together. Examples of both types of compounds have been reported [1–5]. In the first case, the clusters containing the diphosphine ligand show, in general, different metal core geometries from their bis(monophosphine) analogues. This feature enables pairs of skeletal isomers to be obtained [6], which are ruthenium compounds in nearly all the examples described. Os and Fe clusters have been studied less.

This study focuses on the reaction between $[Au_2(diphos)]^{2+}$ (diphos = dppm, dppe, dppp) and the iron anion $[Fe_5C(CO)_{14}]^{2-}$ [7]. The results show the potential of the di-gold cation unit to form new skeletal isomers or to link cluster units if the appropriate stoichiometries and conditions are chosen.

2. Results and discussion

2.1. Electrophilic addition of $[Au_2(diphos)]^{2+}$ to $[Fe_5C(CO)_{14}]^{2-}$ in a 1:1 molar ratio

$(NEt_4)_2[Fe_5C(CO)_{14}]$ reacted in a few minutes with one equivalent of $(ClAu)_2$(dppm) and $TlBF_4$ in tetrahy-

---

* Corresponding author. Fax: +39 521 905557; e-mail: titi@ipruniv.cce.unipr.it

[1] Also corresponding author. Fax: +34 93 4907725; e-mail: orossell@kripto.qui.ub.es

0022-328X/98/$ - see front matter
PII S0022-328X(98)00854-7

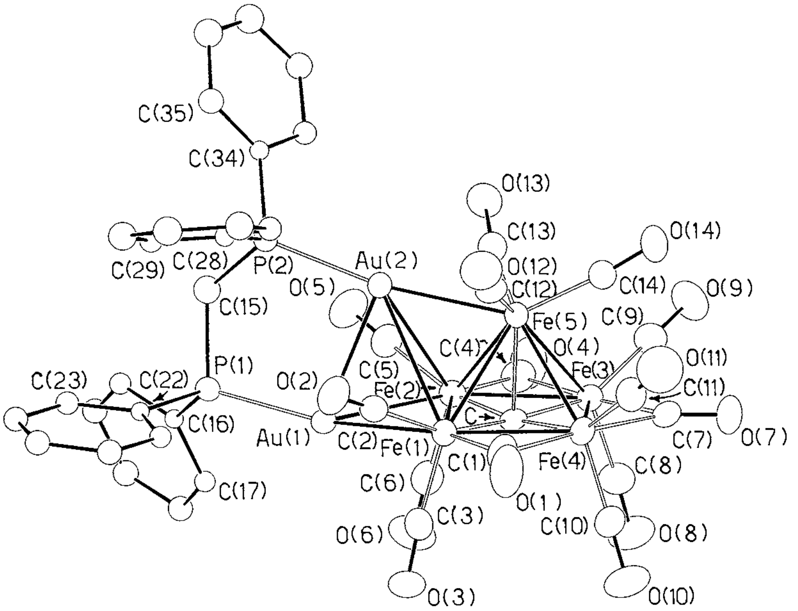

Fig. 1. ORTEP view of the molecular structure of [$Fe_5CAu_2(CO)_{14}$(dppm)] (**1**) together with the atomic numbering scheme. The ellipsoids for the atoms are drawn at the 30% probability level.

drofuran at room temperature to give black crystals of the neutral product [$Fe_5CAu_2(CO)_{14}$(dppm)] (**1**), formulated on the basis of spectroscopic and mass spectrometric data. **1** is air-stable, but its THF solutions decompose slowly under nitrogen at 0°C and give the green product [$Fe_4CAu_2(CO)_{12}$(dppm)] [3]. The ν(CO) IR bands shifted slightly to higher frequencies relative to the starting iron anion, indicating a decrease of electron density on the iron atoms. The FAB(−) mass spectrum of the negative ions was recorded using NBA as the matrix and showed peaks due to the sequential loss of CO groups from the parent anion M^-, ([M−n(CO)]$^-$ ($n = 4–14$)). An X-ray study of the THF solvate of **1** was carried out; the structure of **1** is shown in Fig. 1 together with the atom numbering scheme. Selected bond distances and angles are listed in Table 1. The metal core geometry can be described as a square-based pyramid, with the five Fe atoms lying at the vertices, and a trigonal bipyramid, with the Fe(1), Fe(2) and Au(2) atoms at the vertices of the base and the Au(1) and Fe(5) atoms at the apices, sharing the triangular Fe(1)Fe(2)Fe(5) face. The carbide C atom lies 0.11(1) Å below the Fe(1)Fe(2)Fe(3)Fe(4) mean plane and is at an average distance of 1.879(11) Å from the basal atoms and at a distance of 2.013(9) Å from the apical iron atom. The Au(1) atom bridges the basal Fe(1)–Fe(2) edge, the other three basal edges being bridged by carbonyl ligands (the Fe(1)–Fe(4) and Fe(2)–Fe(3) edges are asymmetrically bridged, whereas the Fe(3)–Fe(4) one is symmetrically bridged).

The bidentate phosphine ligand bridges the Au(1)–Au(2) edge, generating a five-membered ring with a twist conformation. The Au(1)–Au(2) separation of 2.792(1) Å is comparable to those found in other [Au_2(dppm)] containing clusters [1–3] and is almost equal to that found in the ruthenium analogous [$Ru_5CAu_2(CO)_{14}$(dppe)], 2.811(1) Å [4]. The bonding of both gold atoms to the Fe_5 core is extremely asymmetric, as deduced from the gold–iron distances. Thus, the Au(1)–Fe(1) and Au(1)–Fe(2) bond lengths are 2.634(2) Å and 2.799(2) Å, respectively, while those involving Au(2) are 2.592(2) Å [Au(2)–Fe(5)], 3.085(2) Å [Au(2)–Fe(2)] and 3.108(2) Å [Au(2)–Fe(1)], the Fe–Au distances falling outside the range expected for this type of bond [8]. In addition, the Fe–Fe distances of the pentairon skeleton reveal the influence of the coordination of the gold atoms. For example, the values of three Fe–Fe distances of the square base are in the range of 2.561(3)–2.590(3) Å, while that of the gold-bridged edge is 2.861(2) Å. The attachment of the [Au_2(dppm)]$^{2+}$ fragment to the Fe_5 core produces also changes in the bonding mode of the carbonyl ligands [7]b. The most significant is the presence in **1** of the carbonyl ligand C(7)O(7) bridging an edge of the basal plane (C(1)O(1) and C(4)O(4) are semi-bridging).

The structure of **1** compares well with that reported for the ruthenium analogous [$Ru_5CAu_2(CO)_{14}$(dppe)] [4], although the latter is more symmetric because of the less steric constraints produced by the more flexible diphosphine dppe. However, the core geometry of **1** contrasts with that found in [$Fe_5CAu_2(CO)_{14}(PEt_3)_2$] [9], in which a μ_4-$AuPEt_3$ caps the square base of a Fe_5 square pyramid to give a distorted octahedral metal

Table 1
Selected bond distances (Å) and angles (°) for **1**·2THF

Bond lengths (Å)			
Au(1)–Fe(1)	2.634(2)	Au(2)-Fe(1)	3.108(2)
Au(1)–Fe(2)	2.799(2)	Au(2)-Fe(2)	3.085(2)
Au(1)–Au(2)	2.792(1)	Au(2)-Fe(5)	2.592(2)
Fe(1)–Fe(2)	2.861(2)	Fe(1)-Fe(4)	2.585(3)
Fe(1)–Fe(5)	2.699(2)	Fe(2)–Fe(3)	2.590(3)
Fe(2)–Fe(5)	2.695(2)	Fe(3)–Fe(4)	2.561(3)
Fe(3)–Fe(5)	2.644(2)	Fe(4)–Fe(5)	2.626(3)
Fe(1)–C	1.884(10)	Fe(2)–C	1.867(12)
Fe(3)–C	1.871(10)	Fe(4)–C	1.894(12)
Fe(5)–C	2.013(9)	Au(1)–P(1)	2.294(3)
Au(2)–P(2)	2.290(3)	Fe(1)–C(1)	1.859(16)
Fe(2)–C(4)	1.837(13)	Fe(4)–C(1)	2.144(13)
Fe(3)–C(4)	2.138(17)	Fe(4)–C(7)	1.980(12)
Fe(3)–C(7)	1.958(16)		
Bond angles (°)			
Au(2)–Au(1)–Fe(1)	69.8(1)	Au(2)–Au(1)–Fe(2)	67.0(1)
Fe(1)–Au(1)–Fe(2)	63.5(1)	Au(1)–Au(2)–Fe(1)	52.7(1)
Au(1)–Au(2)–Fe(2)	56.6(1)	Au(1)–Au(2)–Fe(5)	99.8(1)
Fe(1)–Au(2)–Fe(2)	55.0(1)	Fe(1)–Au(2)–Fe(5)	55.6(1)
Fe(2)–Au(2)–Fe(5)	55.9(1)	Fe(2)–Au(2)–P(2)	130.0(1)
Fe(1)–Au(1)–P(1)	157.1(1)	Fe(5)–Au(2)–P(2)	170.5(1)
Au(2)–Au(1)–P(1)	98.7(1)	Au(1)–Au(2)–P(2)	89.5(1)
Fe(2)–Au(1)–P(1)	131.6(1)	Fe(1)–Au(2)–P(2)	133.3(1)
Fe(2)–Fe(1)–Fe(4)	86.8(1)	Fe(2)–Fe(3)–Fe(4)	93.4(1)
Fe(1)–Fe(2)–Fe(3)	86.5(1)	Fe(1)–Fe(4)–Fe(3)	93.3(1)
Fe(4)–C–Fe(5)	84.4(1)	Fe(3)–C–Fe(5)	85.7(4)
Fe(2)–C–Fe(5)	87.9(4)	Fe(1)–C–Fe(5)	87.6(4)
Fe(4)–C(1)–O(1)	131.3(11)	Fe(3)–C(4)–O(4)	131.5(11)
Fe(1)–C(1)–O(1)	148.6(12)	Fe(2)–C(4)–O(4)	147.5(12)
Fe(4)–C(7)–O(7)	138.5(10)	Fe(3)–C(7)–O(7)	140.4(11)

arrangement, while the second gold fragment symmetrically bridges an Fe–Fe basal edge. **1** and $[Fe_5CAu_2(CO)_{14}(PEt_3)_2]$ constitute a new example of skeletal isomers [6], produced by the different bonding modes of mono- and diphosphine gold fragments (Scheme 1).

The ^{31}P-NMR spectrum of THF solutions of **1** at 220 K shows two AB spin systems at 41.4 and 43.2 ppm ($^2J(P-P) = 55$ Hz), which collapse at 260 K, and a minor signal at 44.2 ppm. This spectrum can be interpreted in terms of two isomers: one, the most abundant, is consistent with the structure described above and shows fluxional behaviour. The other could consist of a compound exhibiting two symmetrically equivalent gold atoms, although an isomer with two different gold atoms interchanging rapidly can not be ruled out.

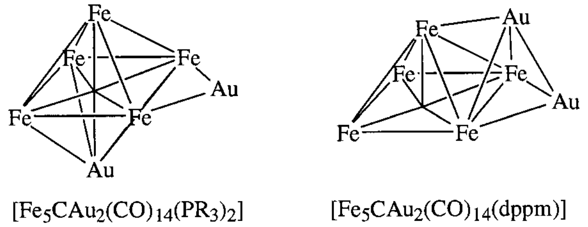

$[Fe_5CAu_2(CO)_{14}(PR_3)_2]$ $[Fe_5CAu_2(CO)_{14}(dppm)]$

Scheme 1.

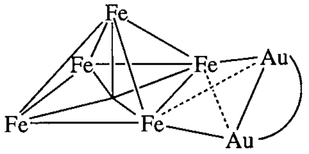

Scheme 2.

In order to propose a structure for this minor isomer, the following considerations were made. The terminal bonding mode Fe–AuP found in the square compound $[Fe_2Au_2(CO)_8(dppm)]$ is characterized by a signal at 40.0 ppm in the ^{31}P-NMR [10]. If the $[Au_2(dppm)]^{2+}$ acts as μ_2 ligand, as occurs in the cluster $[\{Fe_3Au(CO)_{11}\}_2(dppm)]^{2-}$, the chemical shift is 48.3 ppm [5]a. Since the chemical shift in the minor isomer of **1** appears at 44.2 ppm, it seems logical to assign the following structure to this isomer (as is shown in Scheme 2) in which the two iron atoms of the bridged edge and the two gold atoms adopt an intermediate metal array between square and tetrahedral geometry. This bonding mode is analogous to that reported for one isomer of $[Os_4H_2\{AuPPh_3\}_2(CO)_{12}]$ [11].

We have extended our studies to the reaction (1:1) between $[NEt_4]_2[Fe_5C(CO)_{14}]$ and $(ClAu)_2$(diphos) (diphos = dppe and dppp) in order to investigate the influence of the length of the chain on the nature of the resulting cluster.

The ν(CO) IR spectra of the products, $[Fe_5CAu_2(CO)_{14}(diphos)]$ (diphos = dppe, **2**; dppp, **3**), were almost identical to the spectrum found for **1**. The ^{31}P-NMR spectrum showed two signals (56.1, 51.5 and 52.4, 49.2, respectively), indicating the presence of two different uncoupled phosphorus atoms. It is worth noting that no coupling between the two different phosphorous atoms was also observed in the related $[Ru_5CAu_2(CO)_{14}(dppe)]$ [4]. From this data, it is reasonable to assign the same metal skeleton described for **1** to the compounds **2** and **3**.

During these reactions, signals at 30.7 and 24.6 ppm, accompanying those of **2** and **3**, respectively, were detected. Their intensity was reduced when a 0.75 (iron compound): 1 (gold complex) molar ratio was used. As is described next, the signals corresponded to complexes containing two metal cluster units linked by a diphosphine ligand.

2.2. Electrophilic addition of $[Au_2(diphos)]^{2+}$ to $[Fe_5C(CO)_{14}]^{2-}$ in a 1:2 molar ratio

$(ClAu)_2$(diphos) (diphos = dppm, dppe, dppp) was allowed to react with two equivalents of the iron anion in THF at room temperature. According to the stoichiometry of the process, the reaction shown in Scheme 3 takes place.

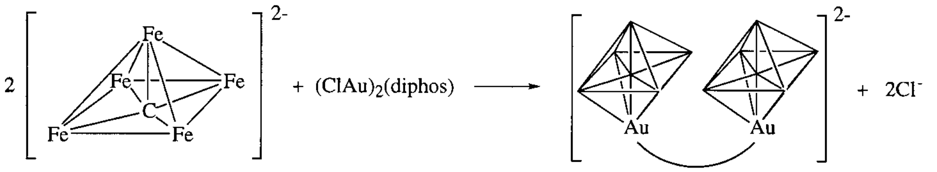

Scheme 3.

The working-up of the solution gave brown crystals of $(NEt_4)_2[\{Fe_5CAu(CO)_{14}\}_2$ (diphos)] (diphos = dppm, **4**; dppe, **5**; dppp, **6**) in moderate yields. The ν(CO) IR pattern was different from that observed for **1-3** and the ^{31}P-NMR spectrum showed only one signal at 31.3, 30.7 and 24.6 ppm for **4-6**, respectively, indicating that a different metal skeleton had been formed. A diphosphine group linking two iron clusters is not rare and some examples have been reported [4,5,10]. The ESMS spectra of these clusters showed clearly both the $M^{2-}/2$ peak and the sequential loss of four carbonyl ligands.

What is not so clear, according to the chemical shift values, distant from those observed for **1-3**, is the coordination mode of the gold atoms in these complexes. One possibility is that the gold atoms in **4-6** were attached to the Fe_5 core by capping the square base of the pyramid, via a μ_4-AuP bonding. Such an interaction has only been found in the clusters $[Fe_5C(CO)_{14}(AuPR_3)_2]$ (R = Et or Ph) [9], as mentioned above. Unfortunately, no NMR data for the latter species were reported, so we were unable to know the expected chemical shift for a μ_4-AuP coordination mode. In order to clarify this point, we treated the $[Fe_5C(CO)_{14}]^{2-}$ anion with two moles of $ClAuPPh_3$ in THF and the ^{31}P-NMR spectrum showed two signals at 32.5 and 55.7 ppm. The values in the literature confirm that the signal at 55.7 ppm falls in the range of complexes exhibiting a μ_2-$AuPPh_3$ unit, while the signal at 32.5 should be assigned to a μ_4-$AuPPh_3$ fragment. Our conclusion is that in **4-6** both gold atoms close the Fe_5 square pyramids to give two distorted Fe_5CAu octahedral arrangements linked by the diphosphine.

As gold fragments could be attached both in a μ_4- and μ_2-manner to a Fe_5C unit, incorporation of a new gold fragment into each octahedral unit, by bridging an edge, to afford a compound with fourteen metal atoms, was attempted. Cluster **6** was reacted with two equivalents of $ClAuPPh_3$ in THF. The analysis of the ^{31}P-NMR spectrum of the solution, proved that two gold-containing compounds were formed: **3** and $[Fe_5C\{AuPPh_3\}_2(CO)_{14}]$ (Scheme 4).

The nature of the resulting products is easily interpreted in terms of a metal ligand redistribution process, which is well known in mercury chemistry [12], but is much less usual for gold clusters [13]. The large volume of the ligands probably facilitates this process by reducing steric hindrance on the metal cluster. This can be seen from the reaction of **6** with the less voluminous $ClAuPMe_3$. Here, the cluster $[\{Fe_5CAu(AuPMe_3)(CO)_{14}\}_2(dppp)]$ (**7**) was obtained (δ (^{31}P) = 52.0, − 12.7 ppm) along with **3** and $[Fe_5C\{AuPMe_3\}_2(CO)_{14}]$ (δ (^{31}P) = 24.8, − 12.4 ppm). All attempts to separate the clusters were unsuccessful. However, the FAB(−) mass spectrum of the solid showed a peak attributable to $[M(\mathbf{7})-CO]^-$ and other peaks corresponding to $[M(\mathbf{3})]^-$, $[Fe_5C\{AuPMe_3\}_2(CO)_{13}]^-$ and $[Fe_5C\{AuPMe_3\}(CO)_{14}]^-$.

3. Experimental

All manipulations were performed under an atmosphere of prepurified N_2 with standard Schlenk techniques, and all solvents were distilled from appropriate drying agents. Infrared spectra were recorded in THF solutions on an FT-IR 520 Nicolet spectrophotometer. $^{31}P\{^1H\}$ -NMR spectra were obtained on a Bruker DXR 250 spectrometer ($\delta(H_3PO_4) = 0.0$ ppm). FAB(−) and Electrospray mass spectra were recorded on a Fisons VG Quattro spectrometer with methanol as the solvent. The complexes $(ClAu)_2$(dppm), $(ClAu)_2$(dppe) and $(ClAu)_2$(dppp) were synthesized and isolated as solids [10] from ClAu(tht) solutions [14] by adding the appropriate amount of the corresponding phosphine. The compound $(NEt_4)_2[Fe_5C(CO)_{14}]$ was synthesized as described previously [7]a.

3.1. Synthesis of $[Fe_5CAu_2(CO)_{14}(diphos)]$ (diphos = dppm (1), dppe (2), dppp (3))

Solid $(ClAu)_2$(dppm) (0.54 g, 0.64 mmol) and $TlBF_4$ (0.37 g, 1.27 mmol) were added to a solution of $(Et_4N)_2[Fe_5C(CO)_{14}]$ (0.60 g, 0.64 mmol) in THF (70 ml). The brown solution became black in a few minutes and was stirred for 1 h at room temperature. Then it was filtered through celite and evaporated to dryness. The residual solid was extracted twice with toluene (2 × 30 ml) and the resulting solution was concentrated to 10 ml and cooled overnight. Black crystals of $[Fe_5CAu_2(CO)_{14}(dppm)]$ were obtained (yield 42%). IR (THF, cm^{-1}): ν(CO) stretch 2056 m, 2019 m, 2004 s, 1982 vs, 1963 m, 1837 w. $^{31}P\{^1H\}$-NMR (220K, THF,

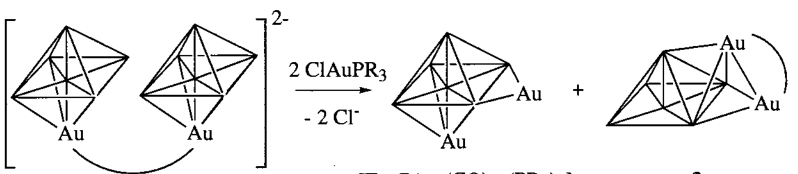

6

$\{Fe_5CAu_2(CO)_{14}(PR_3)_2\}$

3

Scheme 4.

δ(ppm)) 41.4 d, 43.2 d (J(P–P) = 55 Hz, major isomer), 44.2 s (minor isomer). FAB(–) (NBA matrix) (M^- – 4CO): m/z Calc. 1349.1; Found: 1349. Anal. Calc.: C, 32.85; H, 1.51. Found: C, 32.57; H, 1.54.

Compounds **2** and **3** were obtained by a similar procedure, but using a molar ratio of 1:0.75 instead of 1:1. However, the solids precipitated always contained small quantities of other products. $[Fe_5CAu_2(CO)_{14}(dppe)]$ (**2**): IR (THF, cm^{-1}) ν(CO) stretch 2055 m, 2018 m, 2002 s, 1984 vs, 1963 m, 1925 sh, 1833 w. $^{31}P\{^1H\}$-NMR (220K, THF, δ(ppm)) 56.1, 51.5. $[Fe_5CAu_2(CO)_{14}(dppp)]$ (**3**): IR (THF, cm^{-1}): ν(CO) stretch 2054 m, 2020 sh, 2002 s, 1984 vs, 1964 m, 1931 sh, 1831 w. $^{31}P\{^1H\}$-NMR (220K, THF, δ(ppm)) 52.4, 49.2.

*3.2. Synthesis of $[NEt_4]_2[\{Fe_5CAu(CO)_{14}\}_2(diphos)]$ (diphos = dppm (**4**), dppe (**5**), dppp (**6**))*

Details of synthesis of **5** also apply to **4** and **6**. Solid $(ClAu)_2(dppe)$ (0.24 g, 0.27 mmol) and $TlBF_4$ (0.16 g, 0.55 mmol) were added to a solution of $(Et_4N)_2[Fe_5C(CO)_{14}]$ (0.26 g, 0.27 mmol) in THF (30 ml) at room temperature. After stirring for 1 h, another equivalent of $(Et_4N)_2[Fe_5C(CO)_{14}]$ was added. The solution was stirred for a further hour, filtered through celite and concentrated to 10 ml. The addition of 15 ml of diethylether gave dark-brown microcrystals of $[NEt_4]_2$ $[\{Fe_5CAu(CO)_{14}\}_2(dppe)]$ after cooling overnight (yield 68%). IR (THF, cm^{-1}): ν(CO) stretch 2038 m, 1983 vs, 1963 s, 1924 (sh), 1792 w. $^{31}P\{^1H\}$-NMR (240 K, THF, δ(ppm)) 30.7. ESMS (M^-): m/z Calc. 1079.6; Found: 1080. Anal. Calc.: C, 35.74; H, 2.67; N, 1.16. Found: C, 34.88; H, 2.69; N, 1.15. For $[NEt_4]_2[\{Fe_5CAu(CO)_{14}\}_2$ (dppm)] (**4**): IR (THF, cm^{-1}): ν(CO) stretch 2038 m, 1983 vs, 1964 s, 1929 (sh), 1796 w. $^{31}P\{^1H\}$-NMR (240 K, THF, δ(ppm)) 31.2. This compound could not be fully characterized in its solid state because of rapid decomposition. $[NEt_4]_2[\{Fe_5CAu(CO)_{14}\}_2(dppp)]$ (**6**): IR (THF, cm^{-1}): ν(CO) stretch 2037 m, 1980 vs, 1962 s, 1929 (sh), 1791 w. $^{31}P\{^1H\}$-NMR (240 K, THF, δ(ppm)) 24.6. ESMS ($M^{2-}/2$): m/z Calc. 1086.6; Found: 1087. Anal. Calc.: C, 36.03; H, 2.73; N, 1.15. Found: C, 35.89; H, 2.77; N, 1.15.

*3.3. Reaction of $[NEt_4]_2[\{Fe_5CAu(CO)_{14}\}_2(dppp)]$ (**6**) with $ClAuPPh_3$*

To a solution of compound **6** (0.37 g, 0.15 mmol) in THF (30 ml), solid $ClAuPPh_3$ (0.075 g, 0.15 mmol) and $TlBF_4$ (0.044 g, 0.15 mmol) were added and the solution was stirred for 1 h. Then, another 0.15 mmol of $ClAuPPh_3$ and $TlBF_4$ were added, and the black solution stirred for another hour. The $^{31}P\{^1H\}$-NMR of this solution showed four signals (240 K, δ(ppm)): 55.7 and 32.5 ($[Fe_5C\{AuPPh_3\}_2(CO)_{14}]$) and 52.4 and 49.2 (**3**).

*3.4. Reaction of $[NEt_4]_2[\{Fe_5CAu(CO)_{14}\}_2(dppp)]$ (**6**) with $ClAuPMe_3$*

To a solution of compound **6** (0.98 g, 0.40 mmol) in THF (60 ml), solid $ClAuPMe_3$ (0.25 g, 0.81 mmol) and $TlBF_4$ (0.24 g, 0.81 mmol) were added. After 1 h stirring, the $^{31}P\{^1H\}$-NMR of this solution showed peaks at (240 K, δ(ppm)): 52.4 and 49.2 (**3**), 24.8 and – 12.4 ($[Fe_5C\{AuPMe_3\}_2(CO)_{14}]$) and 52.0 and – 12.7 ($[\{Fe_5CAu(AuPMe_3)(CO)_{14}\}_2(dppp)]$ (**7**)). The solution was then concentrated to dryness. The most important peaks observed in the FAB(–) spectrum were (NBA matrix) m/z: 957 ($[Fe_5C\{AuPMe_3\}(CO)_{14}]$), 1202 ($[Fe_5C\{AuPMe_3\}_2(CO)_{13}]$), 1462 (**3**), 2692 (**7**–CO) and 2447 (**7**–$AuPMe_3$).

*3.5. X-ray data collection, structure determination, and refinement for **1** · 2THF*

Crystallographic data are summarized in Table 2. The intensities were collected on a Philips PW 1100 diffractometer using the graphite-monochromated Mo–K_α radiation and the θ–2θ scan technique. 11712 unique reflections were measured with θ in the range 3–27°; 6934 of them, having $I > 2\sigma(I)$, were used in the refinement. One standard reflection was monitored every 100 measurements; no significant decay was noticed over the time of data collection. Intensities were corrected for Lorentz and polarization effects. An empirical correction for absorption was applied (maximum and minimum values for the transmission factors were 1.0 and 0.5147) [15].

Table 2
Crystallographic data for **1**·2THF

Formula	$C_{40}H_{22}Au_2Fe_5O_{14}P_2\cdot 2C_4H_8O$
F_w	1605.93
Crystal system	Triclinic
Space group	$P\bar{1}$
a (Å)	10.160(3)
b (Å)	14.979(4)
c (Å)	18.553(4)
α (°)	73.06(2)
β (°)	86.78(2)
γ (°)	84.88(2)
V (Å^3)	2689(1)
Z	2
$D_{calc.}$ (g cm^{-3})	1.984
$F(000)$	1544
μ (Mo–K$_\alpha$) (cm^{-1})	68.70
λ (cm^{-1})	0.71073
Goodness-of-fit[a]	1.134
$R(F_o)$[b]	0.0527
$R_w(F_o)$[c]	0.0602

[a] $\text{GOF} = [\Sigma\, w(|F_o| - |F_c|)^2/(N_{\text{observns}} - N_{\text{var}})]^{1/2}$.

[b] $R = \Sigma\, ||F_o| - |F_c||/\Sigma|F_o|$.

[c] $R_w = [\Sigma\, w(|F_o| - |F_c|)^2/\Sigma\, w(F_o)^2]^{1/2}$.

The structure was solved by direct (SIR92) [16] and Fourier methods and refined by full-matrix least squares procedures with isotropic thermal parameters; two tetrahydrofurane molecules of solvation were also found (for one of them it was impossible to distinguish the O atom with respect to the carbon atoms). In the last cycles all the non hydrogen atoms, excepting those of the phenyl rings and of the THF molecules of the solvent, were refined anisotropically. The hydrogen atoms, excepting those of the THF molecules, were introduced in the geometrically calculated positions and refined riding on the parent atoms. The final cycles of refinement were carried out on the basis of 490 variables. The highest remaining peak in the final difference map (close to the Au(2) atom) was equivalent to about 2.11 e Å^{-3}. In the final cycles of refinement a weighting scheme $w = K[\sigma^2(F_o) + gF_o^2]^{-1}$ was used; at convergence the K and g values were 0.909 and 0.0013, respectively. The analytical scattering factors, corrected for the real and imaginary parts of anomalous dispersion, were taken from [17]. All calculations were carried out on the GOULD POWERNODE 6040 and ENCORE 91 computers of the 'Centro di Studio per la Strutturistica Diffrattometrica' del C.N.R., Parma, using the SHELX-76 system of crystallographic computer programs [18].

Atomic coordinates, thermal parameters and a complete list of bond distances and angles have been deposited at the Cambridge Crystallographic Data Centre.

Acknowledgements

Financial support was generously provided by the DGICYT (Project PB96-0174), by the CIRIT (Generalitat de Catalunya, Project 1995SGR 00062) and by Consiglio Nazionale delle Ricerche (Rome). G.S. thanks the Ministerio de Educación y Ciencia for a scholarship.

References

[1] I.D. Salter, in: E.W. Abel, F.G.A. Stone, G. Wilkinson (Eds.), Comprehensive Organometallic Chemistry, Ch. 5, vol. 10, Pergamon Press, Elmsford, NY, 1995.
[2] (a) P.J. Bailey, M.A. Beswick, J. Lewis, P.R. Raithby, M.C. Ramírez de Arellano, J. Organomet. Chem., 459 (1993) 293. (b) Z. Akhter, S.L. Ingham, J. Lewis, P.R. Raithby, J. Organomet. Chem., 474 (1994) 165.
[3] O. Rossell, M. Seco, G. Segalés, B.F.G. Johnson, P.J. Dyson, S.L. Ingham, Organometallics 15 (1996) 884.
[4] A.J. Amoroso, A.J. Edwards, B.F.G. Johnson, J. Lewis, M.R. Al-Mandhary, P.R. Raithby, V.P. Saharan, W.T. Wong, J. Organomet. Chem. 443 (1993) 11.
[5] (a) O. Rossell, M. Seco, R. Reina, M. Font-Bardía, X. Solans, Organometallics 13 (1994) 2127. (b) O. Rossell, M. Seco, G. Segalés, J. Organomet. Chem., 503 (1995) 225. (c) P.M.N. Low, A.L. Tan, T.S.A. Hor, Y.S. Wen, L.K. Liu, Organometallics, 15 (1996) 2595.
[6] P. Braunstein, C. de Méric de Bellefon, S.E. Bouaoud, D. Grandjean, J.F. Halet, J.Y. Saillard, J. Am. Chem. Soc. 113 (1991) 5282.
[7] (a) M. Tachikawa, R.L. Geerts and E.L. Muetterties, J. Organomet. Chem., 213 (1981) 11. (b) A. Gourdon and Y. Jeannin, J. Organomet. Chem., 290 (1985) 199.
[8] O. Rossell, M. Seco, G. Segalés, S. Alvarez, M.A. Pellinghelli, A. Tiripicchio, D. de Montauzon, Organometallics 16 (1997) 236.
[9] B.F.G. Johnson, D.A. Kaner, J. Lewis, M.J. Rosales, J. Organomet. Chem. 238 (1982) C73.
[10] S. Alvarez, O. Rossell, M. Seco, J. Valls, M.A. Pellinghelli, A. Tiripicchio, Organometallics 10 (1991) 2309.
[11] B.F.G. Johnson, D.A. Kaner, J. Lewis, P.R. Raithby, M. Taylor, Polyhedron 1 (1982) 105.
[12] L.H. Gade, Angew. Chem. Int. Ed. Engl. 32 (1993) 24.
[13] (a) M. Bardají, N.G. Connelly, M.C. Gimeno, J. Jiménez, P.G. Jones, A. Laguna, M. Laguna, J. Chem. Soc., Dalton Trans. (1994) 1163. (b) E. Cerrada, M.C. Gimeno, J. Jiménez, A. Laguna, M. Laguna, Organometallics, 13 (1994) 1470.
[14] R. Usón, A. Laguna, Organomet. Synth. 3 (1986) 324.
[15] (a) N. Walker, D. Stuart, Acta Crystallogr. A39 (1983) 158. (b) F. Ugozzoli, Comput. Chem. 11 (1987) 109.
[16] A. Altomare, G. Cascarano, C. Giacovazzo, A. Gualiardi, M.C. Burla, G. Polidori, M. Camalli, J. Appl. Crystallogr. 27 (1994) 435.
[17] International Tables for X-ray Crystallography, vol. IV, Kynoch Press, Birmingham, UK, 1974.
[18] G.M. Sheldrick, SHELX-76 Program for Crystal Structure Determination, University of Cambridge, Cambridge, UK, 1976.